From solitons to rogue waves in nonlinear left-handed metamaterials

Yannan Shen,[1] P. G. Kevrekidis,[2] G. P. Veldes,[3,4] D. J. Frantzeskakis,[3] D. DiMarzio,[5] X. Lan,[5] and V. Radisic[5]
[1]*Department of Mathematics and Statistics, California State University, Northridge, California 91330, USA*
[2]*Department of Mathematics and Statistics, University of Massachusetts, Amherst, Massachusetts 01003-4515, USA*
[3]*Department of Physics, National and Kapodistrian University of Athens, Panepistimiopolis, Zografos, Athens 15784, Greece*
[4]*Department of Electronics Engineering, Technological Educational Institute of Central Greece, Lamia 35100, Greece*
[5]*NG Next, Northrop Grumman Corporation, One Space Park, Redondo Beach, California 90278, USA*
(Received 1 December 2016; published 27 March 2017)

In the present work, we explore soliton and roguelike wave solutions in the transmission line analog of a nonlinear left-handed metamaterial. The nonlinearity is expressed through a voltage-dependent, symmetric capacitance motivated by recently developed ferroelectric barium strontium titanate thin-film capacitor designs. We develop both the corresponding nonlinear dynamical lattice and its reduction via a multiple scales expansion to a nonlinear Schrödinger (NLS) model for the envelope of a given carrier wave. The reduced model can feature either a focusing or a defocusing nonlinearity depending on the frequency (wave number) of the carrier. We then consider the robustness of different types of solitary waves of the reduced model within the original nonlinear left-handed medium. We find that both bright and dark solitons persist in a suitable parametric regime, where the reduction to the NLS model is valid. Additionally, for suitable initial conditions, we observe a rogue wave type of behavior that differs significantly from the classic Peregrine rogue wave evolution, including most notably the breakup of a single Peregrine-like pattern into solutions with multiple wave peaks. Finally, we touch upon the behavior of generalized members of the family of the Peregrine solitons, namely, Akhmediev breathers and Kuznetsov-Ma solitons, and explore how these evolve in the left-handed transmission line.

DOI: 10.1103/PhysRevE.95.032223

I. INTRODUCTION

Over the past few years, the study of metamaterials, i.e., artificially engineered structures exhibiting electromagnetic (EM) properties not commonly observed in nature, has seen an explosion of interest [1–4]. An especially intriguing aspect of these metamaterials is their so-called left-handed (LH) nature, which features simultaneously negative effective permittivity ϵ and permeability μ, i.e., the relevant signs of these quantities are opposite to those of conventional right-handed (RH) media. The resulting difference between these two scenarios is that in the LH (RH) regime, the energy and the wave fronts of the EM waves propagate in opposite (same) directions, giving rise to backward (forward)-propagating waves. Consequently, these left-handed metamaterials (LHM) can exhibit negative refraction at microwave [5,6] or optical frequencies [7].

Apart from a classical EM approach involving the study of an effective medium, which can naturally be used to study such metamaterial media [8], transmission line (TL) theory constitutes a convenient framework to analyze their evolutionary dynamics. A TL-based analysis relies on the connection of the EM properties of the medium (ϵ and μ) with the electric elements of the TL unit cell, namely, the serial impedance and the shunt impedance [2]. Equivalent TL models have been used to describe periodic lattices of prototypical magnetic and electric metamaterial structures in the form of split ring resonators (SRRs) and complementary split ring resonators (CSRRs) [9,10]. In this context, each of the SRRs or CSRRs can be analyzed in the form of a corresponding LC circuit, while the whole metamaterial is an array of such circuits, with the coupling between the elements being modeled by a mutual inductance and/or capacitance. The serial impedance and the shunt impedance are directly related to the actual properties of these structures.

In addition to the more standard case of linear LHMs, the study of nonlinear LHMs has been receiving increased attention [11]. Here, the EM properties—such as ϵ and μ (or, equivalently, the serial impedance and the shunt impedance at the TL level)—depend on the intensity of the EM field (equivalently at the TL level, e.g., on the voltage). Practical proposals for the experimental realization of such features involve embedding an array of wires and SRRs into a nonlinear dielectric [12,13] or the insertion of diodes (varactors) into resonant conductive elements, such as the SRRs [14–16]. The interplay of strong dispersion exhibited by left-handed transmission lines with the nonlinear voltage dependence of the group velocity results in unusual dynamical behavior. In this theme, the extensive theoretical studies have led to numerous experimental realizations of features such as pulse propagation [17], envelope soliton formation [18], and the emergence of bright [19] or dark [20] solitons; see also Ref. [21], and the more recent work [22] for soliton generation in active metamaterials. A relevant—but earlier—review of experimental studies can be found in Ref. [23].

In our present considerations, we study a nonlinear left-handed transmission line. In part, we are motivated specifically by the recent development of strongly nonlinear and voltage symmetric barium strontium titanate (BST) thin-film capacitors [24]. We thus consider a nonlinear LHM through a TL approach, which exhibits the symmetric capacitance-voltage dependence. Our aim is to investigate the properties of the nonlinear wave forms that arise and are robustly sustained by this LHM. To gain theoretical insight into this, we utilize a multiscale expansion method that reduces the model, in a self-consistent fashion (up to cubic order in a suitable amplitude parameter), to a nonlinear Schrödinger (NLS) equation [25–27]. We identify regimes, depending on the frequency of the carrier wave, where the NLS equation is

focusing or defocusing. The prototypical soliton solutions of this model, namely, the bright soliton and the dark soliton, are found to be robustly preserved by the transmission line dynamics. However, a more ambitious goal of the present study is to examine whether *rogue wave* (RW) patterns, such as the Peregrine soliton (PS) of the focusing NLS equation, can emerge in the LH transmission line. The only work that we are aware of connecting these two themes (LHMs and RWs) is that of Ref. [28], which focuses on a rather qualitative comparison for very short propagation distances. Here, we actually *engineer* initial data that, at the NLS level, would lead to a PS profile. As a result of the dynamics, we observe both similarities with and differences from what we expect at the NLS level. We discuss these at some length and the impact that the intrinsic features of the LHM system have on the potential emergence and form of the Peregrine-like structure. We do not restrict our considerations to solely this rogue wave pattern; rather, we extend them to additional members of the relevant family of solutions, including the spatially periodic Akhmediev breathers (ABs) and the temporally periodic Kuznetsov-Ma solitons (KMs).

Our presentation is structured as follows. In Sec. II we present the model, discuss the nature of the nonlinearity, and explain the reduction to the NLS setting. In Sec. III, we present prototypical numerical results not only for the bright and dark solitons but also, more importantly, for Peregrine-like solitons and/or rogue waves and related (periodic in space or time) patterns. Finally, in Sec. IV, we summarize our findings and present our conclusions.

II. THE MODEL AND ITS ANALYTICAL CONSIDERATION

Following Ref. [21], we consider the transmission line framework of Fig. 1 in order to model a left-handed TL metamaterial. Assuming that the diode can be emulated by a nonlinear, voltage-dependent capacitance (see below), we can employ Kirchhoff's voltage and current laws for the unit-cell circuit of Fig. 1 and derive (see details in Ref. [21]) the following differential-difference equation for the unknown voltage V_n in the parallel branch at the nth site of the lattice:

$$L_L\frac{d^2}{dt^2}[C_L(U_n)U_n - C_L(U_{n+1})U_{n+1}] - L_L C_R\frac{d^2V_n}{dt^2} - V_n = 0. \quad (1)$$

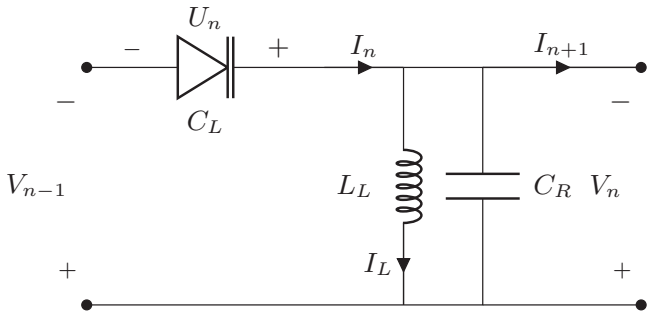

FIG. 1. A sketch of the unit cell of the transmission line emulating the left-handed metamaterial.

Here, U_n is the voltage across the nonlinear capacitance C_L that emulates the in-line BST capacitor (notice that $U_n = V_{n-1} - V_n$), and C_R is the linear shunt capacitance, while L_L represents the inductive elements, connected to the ground; notice that subscripts L and R denote the LH and RH elements of the unit cell circuit. A key feature considered herein is the *symmetric* (contrary to what was the case in Ref. [21]) dependence of the capacitive element on the voltage V. We are motivated by capacitance dependence on voltage results for molecular beam epitaxy grown BST thin films [24]. In particular, we utilize the prototypical symmetric (monotonically increasing with voltage) functional form:

$$C_L(U) = C_0 + \frac{16C_0}{9V_0^2}U^2. \quad (2)$$

Here C_0 is the zero bias capacitance and V_0 has the units of voltage.

As a result of this expansion, Eq. (1) becomes

$$L_L C_0\frac{d^2}{dt^2}(V_{n-1} - 2V_n + V_{n+1}) - L_L C_R\frac{d^2V_n}{dt^2} - V_n + L_L\frac{d^2}{dt^2}\{a[(V_{n-1} - V_n)^3 - (V_n - V_{n+1})^3]\} = 0, \quad (3)$$

where $a = (16/9)(C_0/V_0^2)$. Next, measuring time in units of $1/\omega_0 = \sqrt{L_L C_0}$ and voltage in units of $3V_0/4$, we express Eq. (3) in the following dimensionless form:

$$\frac{d^2}{dt^2}(V_{n-1} - 2V_n + V_{n+1}) - g\frac{d^2V_n}{dt^2} - V_n + \frac{d^2}{dt^2}\{[(V_{n-1} - V_n)^3 - (V_n - V_{n+1})^3]\} = 0, \quad (4)$$

where $g = C_R/C_0$. Below, we use the following typical parameter values: $L_L = 470\ \mu$H, $C_R = 44.8$ pF, $C_0 = 800$ pF, $V_0 = 10$ V, and a unit cell of length $d = 1$ cm (as in Ref. [21]); then, parameter g takes the value $g = 0.056$. Furthermore, the time variable t is measured in units of $\omega_0^{-1} = \sqrt{L_L C_0}$ (with $f_0 = \omega_0/2\pi \approx 260$ kHz); i.e., the time unit is $\approx 0.61\ \mu$s in our simulations below.

To obtain an analytical handle on the nonlinear wave forms that the model of Eq. (4) may possess, we employ a quasicontinuum approximation [29]. In particular, we consider wave forms characterized by a discrete carrier and a slowly varying continuum pulselike envelope and thus seek solutions of Eq. (4) of the form

$$V_n = \sum_{\ell=1}\epsilon^\ell V_\ell(X,T)e^{i\ell(\omega t - kn)} + \text{c.c.}, \quad (5)$$

where V_ℓ are unknown envelope functions, depending on the slow variables:

$$X = \epsilon(n - v_g t), \qquad T = \epsilon^2 t, \quad (6)$$

with v_g being the group velocity, as can be found self-consistently from the linear dispersion relation (see below). Finally, ω and k denote the carrier's frequency and wave number, respectively, and ϵ is a formal small parameter.

Here we should notice that the above ansatz implies that we are assuming a carrier wave of effective linear propagation, as will be more transparent in what follows. This carrier wave is

modulated by a slow envelope that encompasses the nonlinear dynamics of the model. This slow envelope is expected to be governed, as we will see in what follows, by the NLS model. This expansion is a small-amplitude one (i.e., weakly nonlinear), as the relevant control parameter ϵ characterizes the solution amplitude. At the same time, it is a long-wavelength expansion characterizing wide regions of the lattice of size of $1/\epsilon$ and long time scales of the size of $1/\epsilon^2$.

We now present the resulting equations from the multiscale expansion order by order:

$$O(\epsilon^1)\colon \frac{1}{\omega^2} = 2 + g - 2\cos k; \tag{7}$$

$$O(\epsilon^2)\colon v_g = -\omega^3 \sin k; \qquad V_2 = 0; \tag{8}$$

$$O(\epsilon^3)\colon i\partial_T V_1 + P\partial_X^2 V_1 + Q|V_1|^2 V_1 = 0,$$

$$P = \frac{\omega^3}{2}(\cos k - 3\omega^2 \sin^2 k), \quad Q = -24\omega^3 \sin^4(k/2);$$

$$V_3 = \frac{144\omega^2(1+2\cos k)\sin^4(k/2)V_1^3}{1+g-2\cos(3k)}. \tag{9}$$

The first one of these, at O(ϵ), represents the linear dispersion relation of the LHM, which is depicted in the left panel of Fig. 2. Notice that the dispersion relation (7) suggests that there exist two cutoff angular frequencies, namely, an upper one, $\omega_{\max} = 1/\sqrt{g} \approx 4.22$ (corresponding to $k = 0$), and a lower one, $\omega_{\min} = 1/\sqrt{g+4} \approx 0.5$ (corresponding to $k = \pi$), for $g = 0.056$. In physical units, the respective frequencies, are given by $f_{\max} = (2\pi\sqrt{gL_LC_0})^{-1} \approx 1100$ kHz, and $f_{\min} = (2\pi\sqrt{(g+4)L_LC_0})^{-1} \approx 130$ kHz. Notice that the lower cutoff frequency is due to discreteness since, evidently, this frequency vanishes in the continuum limit.

At the next (second) order, the solvability condition leads to the vanishing contribution $V_2 = 0$, as is commonly the case in such multiscale expansions. Furthermore, at the same order, we obtain the group velocity (the velocity of the wave packet's envelope) $v_g = d\omega/dk$, which is not only distinct from the phase velocity $v_p = \omega/k$ but also carries the opposite sign, as per the left-handed nature of the medium; this becomes clear by the form of the dispersion relation shown in the left panel of Fig. 2, which features a negative slope. In other words, $v_p v_g < 0$ (or $kv_g < 0$) means that as a modulated pulse moves forward, the phase evolves in the opposite direction and, hence, motion into the left-handed medium induces the process of phase reversal. Note that the fact that, e.g., $v_g < 0$ and $v_p > 0$ does not violate causality (implying propagation of energy toward the source), as per the arguments of Ref. [30]: the normal to the phase front should not be interpreted as the direction of the group velocity; in fact, the propagation of the front is simply antiparallel to the phase velocity—see discussion and explanations in Refs. [31,32]. This effect is also clearly visible in our simulations (cf. Figs. 3 and 5, as well as the relevant discussion below).

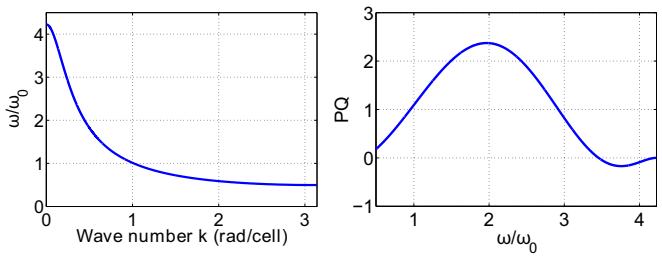

FIG. 2. Left panel: The linear dispersion relation [cf. Eq. (7)]. Right panel: The dependence of the factor PQ (which determines the focusing or defocusing nature of the model) on the frequency ω; see also the text. When $PQ > 0$, the nonlinearity is self-focusing, while for the opposite sign it is self-defocusing.

At the third order, we obtain the NLS equation for V_1. Its dispersion and nonlinearity coefficients, P and Q, respectively, depend on the frequency, but the latter is slaved to the wave number through the dispersion relation. Last, but not least, the third-order reduction and/or decomposition of the solution is also derived.

Considering the abovementioned prototypical values of the relevant parameters, motivated also in part from the experiments of English *et al.* [21], we present PQ as a function of ω in the right panel of Fig. 2, for $g = 0.056$. In the region where the relevant quantity is positive, per the standard general theory of the NLS equation [25–27], the dynamics is associated with a self-focusing scenario that should bear structures like bright solitons, but also potentially Peregrine solitons and related wave forms. In physical units, and for the abovementioned parameter values, the regime of $PQ > 0$ corresponds to the frequency band 130 kHz $\leqslant f \leqslant$ 897 kHz, while the respective wave numbers belong to the interval 0.17 cm^{-1} $\leqslant k \leqslant$ 3.14 cm^{-1}. On the other hand, when $PQ < 0$, we are in a self-defocusing regime where, e.g., dark solitons may arise; the respective frequency and wave number bands in this case are 897 kHz $\leqslant f \leqslant$ 1100 kHz and $0 \leqslant k \leqslant 0.17$ cm^{-1}, respectively. The analytical availability of these wave forms at the NLS level and the explicit form of the transformation allow us to express these potential solutions in the LHM dynamics. As an aside, we note that, for radio frequency, thin-film varactors as in the case of Ref. [24], the value of g may be considerably different. However, we have verified in that case too the existence of self-focusing and self-defocusing frequency ranges and the persistence of the solitary wave structures explored below. Hence, we now turn to direct numerical computations to examine the robustness of such states (and the features thereof) in LHMs.

III. NUMERICAL COMPUTATIONS

In the present section, we explore different wave forms that arise at the level of the NLS model within the realm of the LHM. To do so, we numerically integrate Eq. (4) using a 4th-order Runge-Kutta method and periodic boundary conditions.

A. Bright soliton

It is evident from Fig. 2 that there exists a wide parametric interval of frequencies, for which the effective nonlinearity of the NLS model is self-focusing (i.e., $PQ > 0$). In this case, the prototypical structure that is relevant to explore is the bright soliton. At the level of the leading-order for the voltage, the relevant wave form introduced on the basis of the

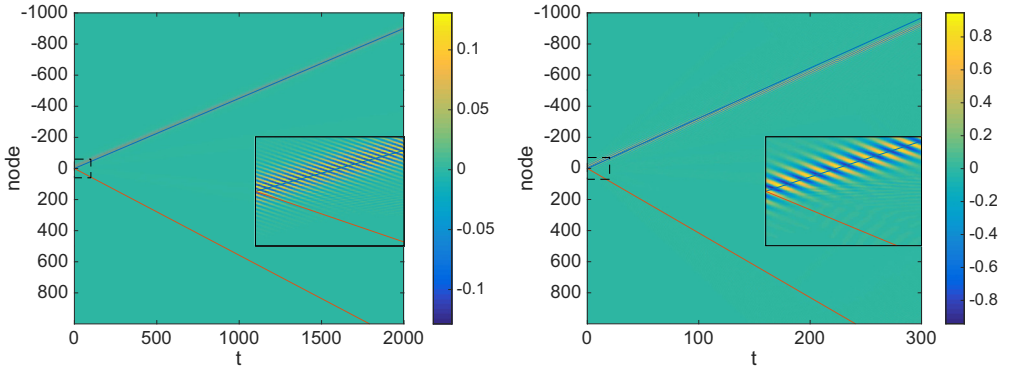

FIG. 3. Contour plots depicting the space (node)-time (t) evolution of a bright soliton propagating through the left-handed medium. Note that $v_p > 0$ and $v_g < 0$, as seen by the slopes of the lower and upper straight lines, respectively. In both panels, insets zooming in the initial stage of the evolution highlight the fact that $v_p v_g < 0$, as is the case for a left-handed medium. The soliton clearly propagates with the prescribed group velocity. The initial data are obtained from the bright soliton solution of Eq. (10) with $u_0 = 1$ and $c = 0$. For the quasicontinuum, long-wavelength approximation, we use $\epsilon = 0.1$, and $(k,\omega) \approx (1.3823, 0.7712)$ in the left panel and $(k,\omega) \approx (0.4650, 1.9305)$ in the right panel; respective values in physical units are $(k, f) \approx (1.3823\ \text{cm}^{-1}, 200\ \text{kHz})$ and $(k, f) \approx (0.4650\ \text{cm}^{-1}, 501\ \text{kHz})$. The maximum soliton amplitudes are 0.93 V (left panel) and 6.7 V (right panel); in both cases, $g = 0.056$.

NLS reduction has the following form:

$$V_1 = \sqrt{\frac{2|P|}{|Q|}}\, u_0\, \mathrm{sech}[u_0(X - 2c|P|T)] \times \exp\left[i\left(cX + \left(u_0^2 - c^2\right)|P|T\right)\right], \qquad (10)$$

where u_0 and c are free O(1) parameters setting the amplitude and/or inverse width and wave number of the soliton, respectively. Utilizing the above expression and reconstructing the initial condition (of the modulated amplitude wave, within the multiscale expansion) based on Eqs. (5)–(9), we can initialize the nonlinear dynamical lattice of Eq. (4) and observe the resulting evolution presented in Fig. 3, for the parameter values discussed above. The dynamics clearly illustrates that for different solutions of varying wave numbers (and frequencies), as well as amplitudes even up to order O(1), we observe the extremely robust propagation of a bright soliton through the LHM. As expected, the multiscale approximation is more accurate for smaller amplitudes, as observed in the left panel of Fig. 3. In the right panel of Fig. 3, for larger amplitude close to O(1), the resulting bright soliton wave packet tends to have a group velocity smaller than that of the theoretical approximation. In this case, a larger fraction of the energy is lost to dispersive wave packet radiation. It is also worth noticing that the insets in both panels of Fig. 3, where a zoom in the initial stage of the evolution is depicted, clearly shows the following: phase fronts travel in opposite direction to the envelope of the wave packet, i.e., $v_p > 0$ and $v_g < 0$, as is expected from the left-handedness of the medium and the discussion in the previous section.

Figure 4 cements the relevant result by illustrating the evolution of the amplitude of the bright soliton (i.e., the maximal absolute value of the voltage) over time. We can see that, although the voltage is modulated by the LH lattice, it is sufficiently robust to be preserved under the long-time evolution. Hence, the bright soliton is an entity able to propagate undistorted over long distances in such left-handed transmission lines.

B. Dark soliton

While in Fig. 2 it can be observed that the interval of frequencies considered is dominated by effective self-focusing dynamics, nevertheless the quantity PQ can change sign.

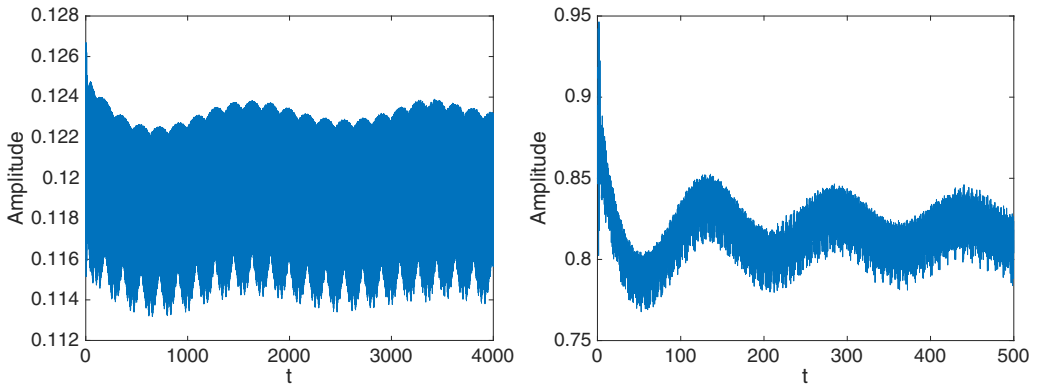

FIG. 4. Amplitude (i.e., maximum voltage) of the bright soliton as a function of time for Fig. 3. Despite the modulation induced by the LH medium, notice the robustness of the bright soliton wave form.

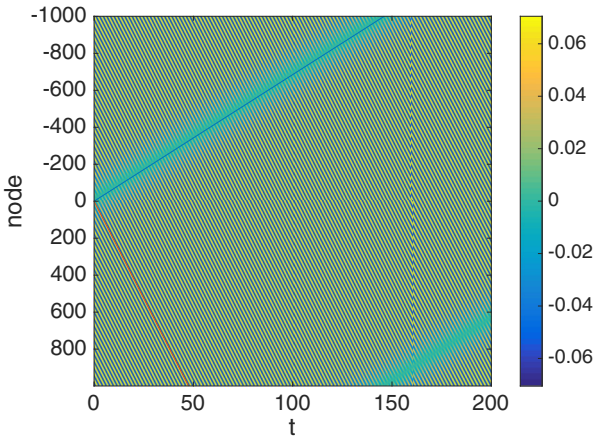

FIG. 5. Dark soliton space-time contour plot evolution for $g = 0.056$. The initial data for the dark soliton solution are obtained on the basis of Eq. (11) using $u_0 = 0.1$, $A = 0$, $B = 1$, $K = 0$, $\epsilon = 0.1$, and $(k,\omega) \approx (0.1649, 3.4681)$ [i.e., $(k, f) \approx (0.1649\,\mathrm{cm}^{-1}, 900\,\mathrm{kHz})$, in physical units]. The background voltage amplitude is 0.53 V. We observe the nearly undistorted propagation of the dark soliton which is now supported by the defocusing NLS model.

Hence, it is natural to explore the potential for the formation of dark soliton states, voltage dips on top of a carrier wave (voltage) background. The relevant functional form of the dark soliton solution of Eq. (9) for $PQ < 0$ reads as follows:

$$V_1 = \sqrt{\frac{2|P|}{|Q|}} u_0 [B \tanh(u_0 B X) + i A] \times \exp\left[i\left(KX - \left(2u_0^2 + K^2\right)|P|T\right)\right], \tag{11}$$

where u_0 and K are the background amplitude and the wave number of the carrier, while B and A set the amplitude ("darkness") and velocity of the soliton, respectively (note that $A^2 + B^2 = 1$). We have once again used Eq. (11) and the long-wavelength multiscale expansion machinery of Eqs. (5)–(9) to construct a suitable initial condition for the dynamical lattice of Eq. (4). The result in the space-time contour plot evolution of the voltage is shown in Fig. 5. In this case too, although the entire background is excited, we can observe that the voltage dip propagates essentially undistorted over a long propagation distance, following the prescribed (through the analysis) group velocity. It is also noted that, as in the case of the bright soliton, phase fronts travel in the opposite direction to the envelope of the wave packet, i.e., $v_p > 0$ and $v_g < 0$, as discussed in the previous section.

We now turn to the Peregrine soliton.

C. Peregrine soliton

The study of solutions of the focusing NLS involving extreme events (associated with rogue waves) has had a long and time-honored history through the works of Peregrine [33], Kuznetsov [34], Ma [35], Akhmediev *et al.* [36], and Dysthe and Trulsen [37]; see also the reviews [38–40]. However, it has been the recent experiments in a wide range of areas that has significantly propelled the amount of interest in the related wave structures. In particular, relevant experiments reporting observations of rogue waves have emerged in the study of nonlinear optics [41–45], mode-locked lasers [46], superfluid helium [47], hydrodynamics [48–50], Faraday surface ripples [51], parametrically driven capillary waves [52], and plasmas [53].

In our problem, given the NLS reduction, we can utilize the Peregrine soliton solution of the focusing NLS model in the following form,

$$V_1 = \sqrt{\frac{2|P|}{|Q|}} u_0 \left(1 - \frac{4\left(1 + 4iu_0^2|P|T\right)}{1 + 4u_0^2 X^2 + 16u_0^4|P|^2T^2}\right) \times \exp(i2u_0^2|P|T), \tag{12}$$

(here, as before, u_0 is the amplitude of the background carrier wave) to reconstruct the initial condition of a wave form to be introduced in Eq. (4) via Eqs. (5)–(9).

We initialize the relevant wave form at a time well before the formation of its maximum and observe its full evolution. We do this both for a smaller amplitude case, where the reduction should be more representative of the true NLS dynamics, and for a larger amplitude one. Figure 6 shows a Peregrine soliton example with a small amplitude; $\epsilon = 0.1$ is used here. The dynamical evolution illustrates that the number of peaks progressively increases; i.e., while there is the emergence of the fundamental peak associated presumably with the Peregrine soliton, for longer times an evolution somewhat reminiscent of modulational instability and the formation of a more complex pattern consisting of multiple breathing solitary wave entities appear to emerge. It is worthwhile to mention (also in connection with the results that follow) that the growth towards the formation of the Peregrine soliton is not monotonic (as is expected by the exact solution). Rather, there is a slight interval

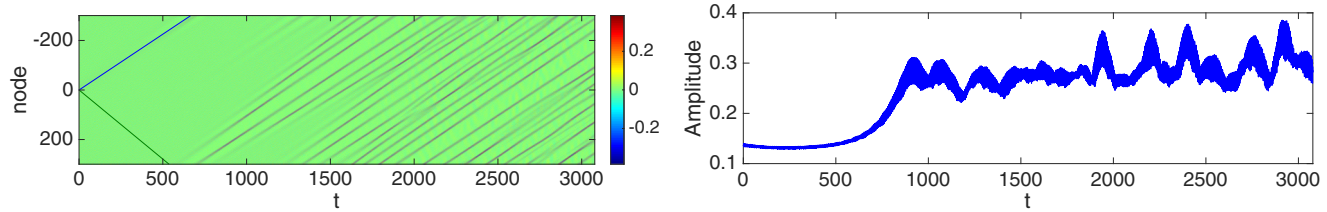

FIG. 6. Evolution of a Peregrine soliton in the left-handed metamaterial lattice, for parameter values as in the left panel of Fig. 3. The left panel shows the space-time contour plot of the lattice, while the right panel shows the evolution of the maximum voltage amplitude. Note that, in physical units, the initial and maximum values of the voltage are 1.03 and 2.7 V, respectively.

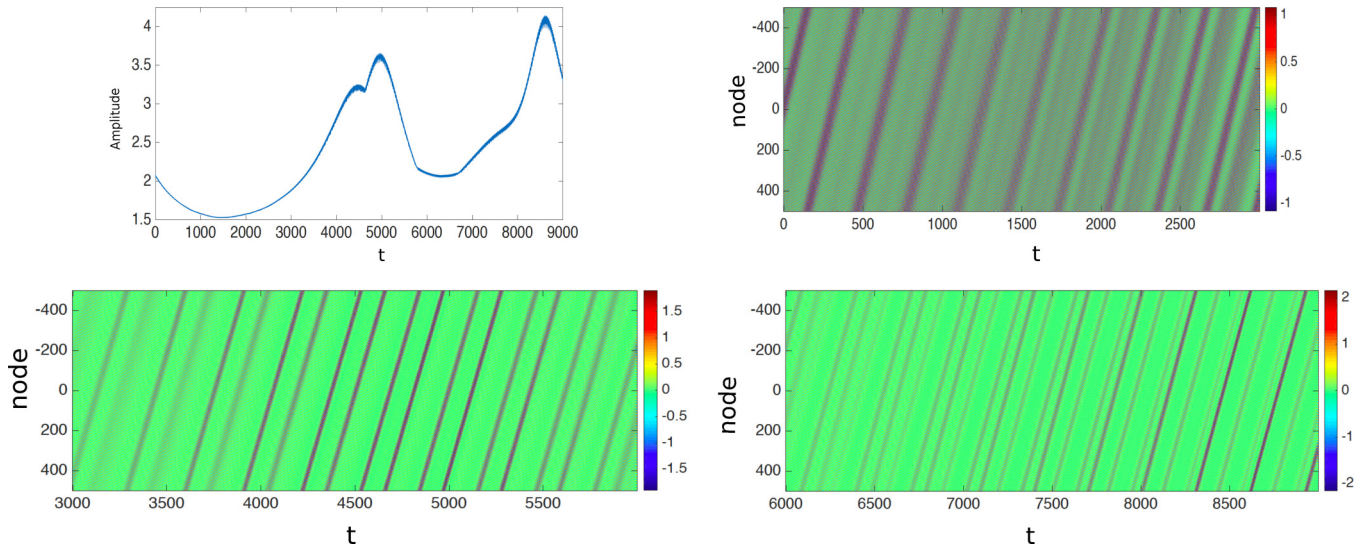

FIG. 7. Evolution through the left-handed metamaterial lattice of a Peregrine soliton for $\omega = 1.926$ ($f \approx 503$ kHz in physical units) and $g = 0.056$. Here, Eq. (12) is utilized to obtain the initial condition in the original variables. The top left panel shows the evolution of the solution's maximum. The top right, bottom left, and bottom right panels show a very long space-time contour plot for the evolution of the voltage. For the formation of a large-amplitude (extreme) event and the subsequent splitting, see details in the text.

of amplitude decay before the growth, ultimately leading to the emergence of the extreme event.

Figure 7 corresponds to a case of substantially larger initial voltage, where we expect the small amplitude reduction to no longer be valid. This case also illustrates a number of similarities and differences with respect to the original NLS model. In the NLS, a monotonic growth of the "bulge" develops, leading to the peak of the Peregrine soliton (which thus seems to "appear out of nowhere and disappear without a trace" [54]). Here, in our lattice, the growth still occurs, yet it involves a decay stage before the growth stage leading to the peak. After the formation of the peak, a somewhat unconventional sequence arises in the time evolution of the maximum. While, that is, we expect decay anew, this decay occurs only briefly, with another growth stage and a sharp (in fact, even sharper than the previous one) peak emerging. The top right panel of Fig. 7 illustrating the space-time evolution until $t = 3000$ sheds light on this feature. In particular, what happens is that the original "wider" wave form splits into two narrower peaks, which evolve rather independently. At the level of the amplitude, further evolution leads to decay and then once again to growth (the latter time developing even higher voltage amplitudes). Once again, the contour plots of the bottom panels for considerably larger times reveal the explanation: in a similar way as the single wave eventually grows and splits into two, the two subsequently proceed to split, forming an additional one. This way, the number of wave structures appears to be increasing over time. While this is not consonant with the exact solution of the Peregrine soliton in NLS, we should note that it is reminiscent of an evolution leading to a progressive increase in the number of peaks in the recent work [55]. Furthermore, although it is far more ordered, it carries some of the breathing characteristics of the smaller amplitude case in Fig. 6.

Thus, summarizing our findings, there exist definite similarities between the NLS reduction and the dynamics of the LHM, including the formation of extreme wave patterns. Nevertheless, there are also notable differences, such as the nonmonotonic growth or the breakup of the latter initial profile into multiple waves, which—especially at large amplitudes—seems to be more complex than what may be expected on the basis of the NLS reduction.

D. Akhmediev breathers and Kuznetsov-Ma solitons

As is well known [34–36], the Peregrine soliton can be viewed as a low wave number or a low-frequency limit of a generalized family of solutions including on the one hand the Akhmediev breathers and on the other Kuznetsov-Ma solitons, respectively. Both these structures are solutions of the focusing NLS equation and can be written in a single form as

$$V_1 = \sqrt{\frac{2|P|}{|Q|}}\left[1 + \frac{2(1-2a)\cosh(2b|P|T) + ib\sinh(2b|P|T)}{\sqrt{2a}\cos(KX) - \cosh(2b|P|T)}\right]\exp(2i|P|T), \tag{13}$$

where $b = \sqrt{8a(1-2a)}$ and $K = 2\sqrt{1-2a}$. For $0 < a < 0.5$ the solution is referred to as an Akhmediev breather, with period $2\pi/K$ in X. For $a > 0.5$, K and b become imaginary, thus the solution is periodic with period $\pi/(b|P|)$ in T and Eq. (13) represents a Kuznetsov-Ma soliton. In the limit of $a \to 0.5$, these periods (spatial and temporal, respectively) approach ∞ and Eq. (13) has as a limiting case the Peregrine soliton solution of NLS. Given the NLS reduction, we can

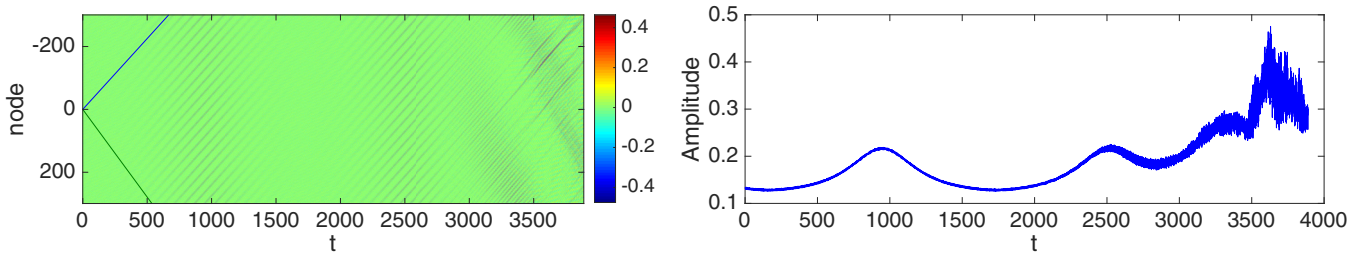

FIG. 8. Evolution through the left-handed metamaterial lattice of an Akhmediev breather for $f \approx 200$ kHz and $g = 0.056$. We use Eq. (13) with $a = 0.1131$ to obtain the initial condition in the original variables. Here, we start from the time before the formation of the maximum amplitude of the Akhmediev breather. Once again, the space-time contour plots of the voltage (left) and of the maximal evolution of the voltage amplitude over time (right) are shown. In this case, in physical units, the initial and maximum values of the voltage are 0.98 and 3.6 V, respectively.

utilize Eq. (13) with different values of a to reconstruct these types of initial conditions of Eq. (4) via Eqs. (5)–(9).

Figure 8 shows the dynamics of the LHM with the initial data taken from Eq. (13) for $a = 0.1131$, in the regime where the solution is anticipated to evolve into an Akhmediev breather. As in the Peregrine examples, our initialization time is before the formation of the maximum amplitude of the Akhmediev breather. We observe for the amplitude that, instead of growing to form the relevant pattern and subsequently decaying to a constant background forever as is prescribed by the NLS equation, it oscillates until the humps become irregular. Such a manifestation is, once again, somewhat reminiscent of modulational instability and the subsequent formation of more highly localized wave forms. As a complementary simulation, we also used the initial data of the LHM with $T = 0$ of Eq. (13), i.e., at the maximum amplitude of the Akhmediev breather. Then we observe that, besides the group velocity being slightly slower than the theoretical prediction, the amplitude for each individual hump actually oscillates simultaneously for a while until around $t = 1400$ with a much shorter period in Fig. 9 than in Fig. 8. Eventually, however, in this case too the oscillatory pattern destabilizes and leads to an irregular profile of the energy distribution over the lattice, which also features occasional sharper localization phenomena.

Figure 10 shows the dynamical evolution of the LHM with initial data from Eq. (13) at $a = 0.9$, in the regime of the Kuznetsov-Ma soliton. Since the Kuznetsov-Ma soliton is time periodic, this time we start from $T = 0$, i.e., at the maximum amplitude of the Kuznetsov-Ma soliton. We observe that the single hump splits into two humps at a very early stage, one with group velocity considerably smaller than the theoretical prediction and the other one with a group velocity larger than the one suggested by the NLS reduction. This procedure keeps cascading for the duration of our numerical integration, in a way once again reminiscent of the pattern formation via modulational instability. In fact, even in the case of the Peregrine soliton, an initialization at the maximum amplitude leads to the observation of similar dynamics with a splitting at an early stage. Besides that, as in the right panel of Fig. 10, we observe an oscillating amplitude, which is similar initially to the Kuznetsov-Ma soliton, until the interactions with the apparently unstable background disrupt its nearly periodic evolution.

IV. CONCLUSIONS AND FUTURE CHALLENGES

In the present work, we have revisited the study of left-handed transmission line metamaterials, motivated by the consideration of strong voltage symmetric nonlinearities demonstrated for epitaxially fabricated BST capacitors. Upon introducing the relevant theoretical model, we have argued that its dispersive character renders it suitable for a carrier-envelope decomposition and an associated multiple scales reduction. This approach, as is customary in such models, leads to a nonlinear Schrödinger (NLS) equation which is a host to a diverse array of coherent wave form structures.

We illustrated that focusing as well as defocusing nonlinearities can be engineered on the basis of varying the frequency (or wave number) of the carrier wave. In the case of effectively self-defocusing nonlinearities, we observed the robust propagation of dark solitons in the system. In a similar way, for focusing nonlinearities, bright solitons were found to be generically robust. What was most interesting, however, was

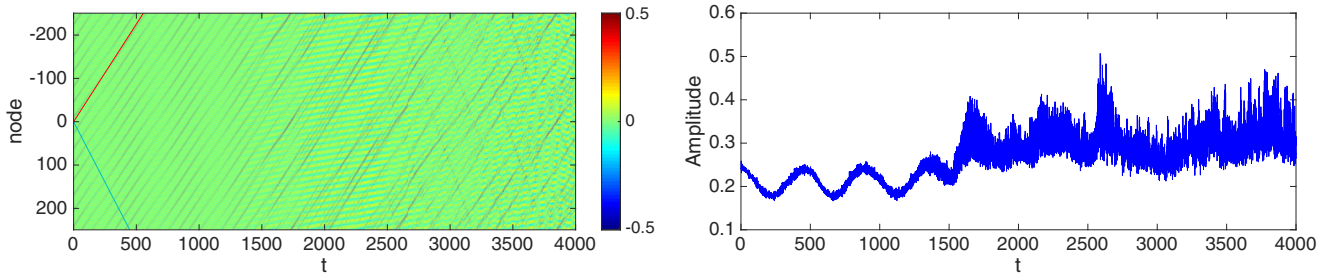

FIG. 9. Same as in Fig. (8) but for initial data using Eq. (13) at $T = 0$.

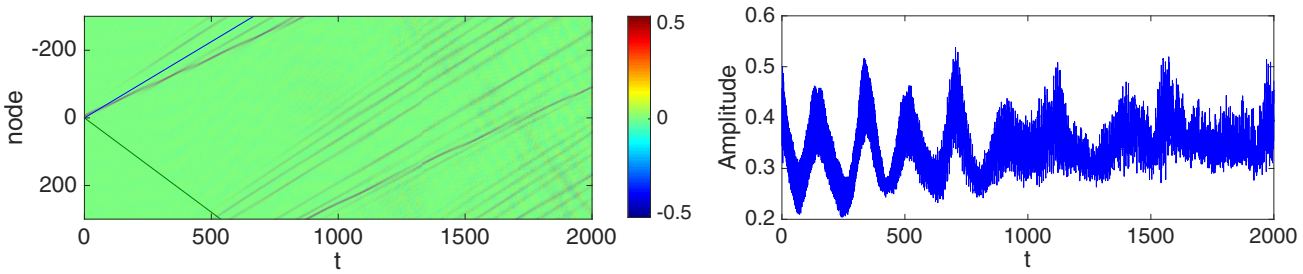

FIG. 10. Evolution through the left handed metamaterial lattice of a Kuznetsov-Ma soliton for $f \approx 200$ kHz and $g = 0.056$. The solution of Eq. (13) with $a = 0.9$ is utilized to obtain the initial condition in the original variables. The same diagnostics, namely, voltage space-time contour plot (left panel) and maximal voltage vs. time (right panel) are depicted. In this case, in physical units, the initial and maximum values of the voltage are 3.4 and 4.0 V, respectively.

the possibility for producing extreme wave form events, in the form of rogue waves (Peregrine solitons, but also Akhmediev breathers and Kuznetsov-Ma solitons) for such left-handed media. We observed that such events do arise through suitable initial conditions, motivated by the NLS reduction. In particular, these extreme wave forms demonstrated both similarities with and differences from the standard Peregrine soliton case, the differences being the nonmonotonic growth, as well as the subsequent (to the formation of the peak) emergence of multiple peaks signaling, arguably, the modulational instability of the background. Similarly to the case of the Peregrine soliton, the Akhmediev breather and the Kuznetsov-Ma soliton preserved some of their characteristics such as the approximate spatial or temporal (respectively) periodicity, but at the same time, they also manifested nontrivial perturbations in both space and time, due to the modulational features of their corresponding background.

The results of the present study stimulate numerous further explorations within this general area of the interplay of nonlinearity and left-handed media, especially around the subject of extreme events and rogue waves. At the one-dimensional (1D) level, it may be well worthwhile to examine more general lattices, potentially also involving right-handed parasitic elements (as in Ref. [21]), or more broadly composite left-handed and right-handed element chains as, e.g., in Ref. [56]. A natural question is to what degree Peregrine type patterns may persist in such settings. Another major direction for future investigations is that of exploring the role of dimensionality. In particular, recent studies have explored even experimentally the role of geometry (e.g., square vs triangular, etc.) in transmission line implementations of two-dimensional (2D) lattices [57]. It would be especially relevant to consider left handed such media and particularly the possibility of inducing 1D (or even more intriguingly 2D) extreme events in the latter. Such studies are currently in progress and will be reported in future publications.

ACKNOWLEDGMENTS

P.G.K., G.P.V., and D.J.F. acknowledge that this publication was made possible by NPRP Grant No. 9-329-1-067 from the Qatar National Research Fund (a member of the Qatar Foundation). P.G.K. also gratefully acknowledges the support of Grant No. NSF-PHY-1602994, the Alexander von Humboldt Foundation, the Stavros Niarchos Foundation via the Greek Diaspora Fellowship program, and the ERC under FP7, Marie Curie Actions, People, International Research Staff Exchange Scheme (IRSES-605096). We would like to thank S. Stemmer and R. York from the University of California at Santa Barbara for providing the BST capacitor model.

[1] G. V. Eleftheriades and K. G. Balmain (eds.), *Negative-Refraction Metamaterials: Fundamental Principles and Applications* (Wiley, New York, 2005).
[2] C. Caloz and T. Itoh, *Electromagnetic Metamaterials: Transmission Line Theory and Microwave Applications* (Wiley, New York, 2006).
[3] R. Marqués, F. Martín, and M. Sorolla, *Metamaterials with Negative Parameters: Theory, Design, and Microwave Applications* (John Wiley and Sons, New York, 2008).
[4] D. R. Smith, J. B. Pendry, and M. C. K. Wiltshire, Science **305**, 788 (2004); J. B. Pendry and D. R. Smith, Phys. Today **57**, 37 (2004)
[5] D. R. Smith, W. J. Padilla, D. C. Vier, S. C. Nemat-Nasser, and S. Schultz, Phys. Rev. Lett. **84**, 4184 (2000).
[6] D. R. Smith and N. Kroll, Phys. Rev. Lett. **85**, 2933 (2000); A. Shelby, D. R. Smith, and S. Schultz, Science **292**, 77 (2001).
[7] V. M. Shalaev, Nat. Photonics **1**, 41 (2007).
[8] J. A. Kong, *Electromagnetic Wave Theory* (Wiley, New York, 1990).
[9] E. Shamonina, V. A. Kalinin, K. H. Ringhofer, and L. Solymar, Electron. Lett. **38**, 371 (2002); R. R. A. Syms, E. Shamonina, V. Kalinin, and L. Solymar, J. Appl. Phys. **97**, 064909 (2005).
[10] M. Beruete, F. Falcone, M. J. Freire, R. Marqus, and J. D. Baena, Appl. Phys. Lett. **88**, 083503 (2006).
[11] M. Lapine, I. V. Shadrivov, and Yu. S. Kivshar, Rev. Mod. Phys. **86**, 1093 (2014).
[12] A. A. Zharov, I. V. Shadrivov, and Yu. S. Kivshar, Phys. Rev. Lett. **91**, 037401 (2003).
[13] V. M. Agranovich, Y. R. Shen, R. H. Baughman, and A. A. Zakhidov, Phys. Rev. B **69**, 165112 (2004).
[14] M. Lapine, M. Gorkunov, and K. H. Ringhofer, Phys. Rev. E **67**, 065601 (2003).
[15] B. Wang, J. Zhou, T. Koschny, and C. M. Soukoulis, Opt. Express **16**, 16058 (2008).

[16] D. A. Powell, I. V. Shadrivov, and Yu. S. Kivshar, Appl. Phys. Lett. **95**, 084102 (2009).
[17] A. B. Kozyrev, H. Kim, A. Karbassi, and D. W. van der Weide, Appl. Phys. Lett. **87**, 121109 (2005).
[18] A. B. Kozyrev and D. W. van der Weide, Appl. Phys. Lett. **91**, 254111 (2007).
[19] J. Ogasawara and K. Narahara, IEICE Electronic Express **7**, 608 (2010).
[20] Z. Wang, Y. Feng, B. Zhu, J. Zhao, and T. Jiang, J. Appl. Phys. **107**, 094907 (2010).
[21] L. Q. English, S. G. Wheeler, Y. Shen, G. P. Veldes, N. Whitaker, P. G. Kevrekidis, and D. J. Frantzeskakis, Phys. Lett. A **375**, 1242 (2011).
[22] A. B. Kozyrev, I. V. Shadrivov, and Yu. S. Kivshar, Appl. Phys. Lett. **104**, 084105 (2014).
[23] A. B. Kozyrev and D. W. van der Weide, J. Phys. D: Appl. Phys. **41**, 173001 (2008).
[24] C. J. G. Meyers, C. R. Freeze, S. Stemmer, and R. A. York, Appl. Phys. Lett. **109**, 112902 (2016)
[25] C. Sulem and P. L. Sulem, *The Nonlinear Schrödinger Equation* (Springer-Verlag, New York, 1999).
[26] M. J. Ablowitz, B. Prinari, and A. D. Trubatch, *Discrete and Continuous Nonlinear Schrödinger Systems* (Cambridge University, Cambridge, England, 2004).
[27] P. G. Kevrekidis, D. J. Frantzeskakis, and R. Carretero-González, *The Defocusing Nonlinear Schrödinger Equation* (SIAM, Philadelphia, 2015).
[28] B. G. Onana Essama, J. Atangana, F. Biya Motto, B. Mokhtari, N. Cherkaoui Eddeqaqi, and T. C. Kofane, J. Mod. Opt. **61**, 1002 (2014).
[29] M. Remoissenet, *Waves Called Solitons* (Springer-Verlag, Berlin, 1999).
[30] P. M. Valanju, R. M. Walser, and A. P. Valanju, Phys. Rev. Lett. **88**, 187401 (2002).
[31] J. B. Pendry and D. R. Smith, Phys. Rev. Lett. **90**, 029703 (2003).
[32] J. Pacheco, Jr., T. M. Grzegorczyk, B.-I. Wu, Y. Zhang, and J. A. Kong, Phys. Rev. Lett. **89**, 257401 (2002).
[33] D. H. Peregrine, J. Aust. Math. Soc. Ser. B **25**, 16 (1983).
[34] E. A. Kuznetsov, Sov. Phys. Dokl. **22**, 507 (1977).
[35] Ya. C. Ma, Stud. Appl. Math. **60**, 43 (1979).
[36] N. N. Akhmediev, V. M. Eleonskii, and N. E. Kulagin, Theor. Math. Phys. **72**, 809 (1987).
[37] K. B. Dysthe and K. Trulsen, Phys. Scr., T **82**, 48 (1999).
[38] Z. Yan, J. Phys.: Conf. Ser. **400**, 012084 (2012).
[39] P. T. S. DeVore, D. R. Solli, D. Borlaug, C. Ropers, and B. Jalali, J. Opt. **15**, 064001 (2013).
[40] M. Onorato, S. Residori, U. Bortolozzo, A. Montinad, and F. T. Arecchi, Phys. Rep. **528**, 47 (2013).
[41] D. R. Solli, C. Ropers, P. Koonath, and B. Jalali, Nature (London) **450**, 1054 (2007).
[42] B. Kibler *et al.*, Nat. Phys. **6**, 790 (2010).
[43] B. Kibler *et al.*, Sci. Rep. **2**, 463 (2012).
[44] J. M. Dudley, F. Dias, M. Erkintalo, and G. Genty, Nat. Photonics **8**, 755 (2014).
[45] B. Frisquet *et al.*, Sci. Rep. **6**, 20785 (2016).
[46] C. Lecaplain, Ph. Grelu, J. M. Soto-Crespo, and N. Akhmediev, Phys. Rev. Lett. **108**, 233901 (2012).
[47] A. N. Ganshin, V. B. Efimov, G. V. Kolmakov, L. P. Mezhov-Deglin, and P. V. E. McClintock, Phys. Rev. Lett. **101**, 065303 (2008).
[48] A. Chabchoub, N. P. Hoffmann, and N. Akhmediev, Phys. Rev. Lett. **106**, 204502 (2011).
[49] A. Chabchoub, N. Hoffmann, M. Onorato, and N. Akhmediev, Phys. Rev. X **2**, 011015 (2012).
[50] A. Chabchoub and M. Fink, Phys. Rev. Lett. **112**, 124101 (2014).
[51] H. Xia, T. Maimbourg, H. Punzmann, and M. Shats, Phys. Rev. Lett. **109**, 114502 (2012).
[52] M. Shats, H. Punzmann, and H. Xia, Phys. Rev. Lett. **104**, 104503 (2010).
[53] H. Bailung, S. K. Sharma, and Y. Nakamura, Phys. Rev. Lett. **107**, 255005 (2011).
[54] N. Akhmediev, J. M. Soto-Crespo, and A. Ankiewicz, Phys. Lett. A **373**, 2137 (2009).
[55] E. G. Charalampidis, J. Cuevas-Maraver, D. J. Frantzeskakis, and P. G. Kevrekidis, arXiv:1609.01798.
[56] G. P. Veldes, J. Cuevas, P. G. Kevrekidis, and D. J. Frantzeskakis, Phys. Rev. E **88**, 013203 (2013).
[57] L. Q. English, F. Palmero, J. F. Stormes, J. Cuevas, R. Carretero-González, and P. G. Kevrekidis, Phys. Rev. E **88**, 022912 (2013).